

# Training distribution determines the ceiling of drug-blind cancer sensitivity prediction

Taekyung Heo

taekyung.cs@gmail.com

## Abstract

Precision oncology requires predicting which drugs will suppress a specific tumor from its molecular profile, but drug-blind sensitivity prediction has plateaued despite increasingly complex drug representations. Here we show that this stagnation reflects a metric artifact rather than a representational bottleneck. The standard benchmark, global Pearson  $r$ , is dominated by between-drug potency differences that a trivial drug-mean predictor captures without any cell-specific learning. Per-drug Pearson  $r$ , which isolates within-drug cell ranking, reveals that no drug encoding improves over cell-only features across four independent datasets. A controlled experiment channeling mechanism-of-action identity as either a drug feature or a training-distribution constraint identifies the cause. Supplying MoA as a feature yields negligible benefit, whereas using it to stratify training raises per-drug  $r$  substantially for targeted kinase inhibitors, because pan-cancer co-training suppresses pathway-specific sensitivity signals. Mechanism-stratified training and response matching from pilot observations provide two deployable strategies that together recover the principal sources of predictive gain in drug-blind sensitivity prediction.

## Introduction

Predicting which drugs will suppress a specific tumor from its molecular profile is the central computational challenge of precision oncology<sup>1,2</sup>. In the drug-blind setting, where models must generalize to compounds absent from training, a decade of increasingly sophisticated drug encoders has converged on a ceiling of global Pearson  $r \approx 0.45$ – $0.55$ <sup>3,4</sup>, raising the question of whether drug

representations are fundamentally limited or merely underspecified.

Recent evidence reframes this debate. A drug-mean oracle achieves global Pearson  $r = 0.85$  on GDSC<sup>5</sup>, and removing the drug branch from deep models does not degrade performance in cancer-blind evaluation<sup>6</sup>. We show that the same null extends to the drug-blind setting under per-drug  $r$  (Fig. 2b). These observations indicate that global  $r$  conflates two signals: between-drug potency ranking and within-drug cell ranking. Per-drug Pearson  $r$ , computed within each test drug across cell lines, isolates cell ranking and more directly addresses the clinical question of which patients respond to a given compound.

Under per-drug  $r$ , no drug representation produces more than a negligible improvement over cell-only features. This holds for structural encodings (Morgan fingerprints<sup>7</sup>, ChemBERTa<sup>8</sup>), functional encodings (LINCS L1000 perturbation signatures<sup>9</sup>), and drug-target vectors, and is confirmed independently in drug-blind evaluation<sup>10,11</sup> and in the drug-seen regime<sup>12</sup>. We replicate the null in both ridge regression and an 11.7M-parameter Transformer encoder. Reported ceilings above this null are explained by test-set checkpoint selection in several prominent models, consistent with widespread evaluation leakage documented across the field<sup>13</sup>.

Here, we address whether this failure is informational (the model lacks the right drug encoding) or distributional (the model trains on the wrong drugs). A controlled experiment channels the same mechanism of action (MoA) information through two routes: as a drug feature or as a training distribution (Fig. 3). Training distribution alignment dominates representation across both ridge

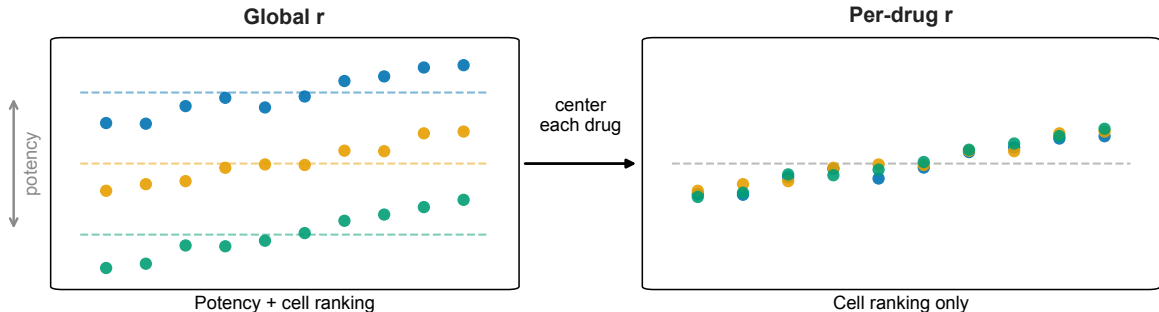


**Fig. 1 — Global  $r$  conflates two independent signals. Per-drug  $r$  isolates within-drug cell ranking.** Three drugs (colored) span different mean sensitivity levels (potency) while sharing the same relative cell-line ordering. Global Pearson  $r$  (left) reflects both potency differences and cell ranking. Removing each drug’s mean (per-drug  $z$ -scoring) yields per-drug  $r$  (right), which isolates cell ranking.

regression and an 11.7M-parameter Transformer encoder, and two practical strategies exploit this to improve within-drug cell ranking across independent datasets.

## Results

### Per-drug evaluation reveals a hidden ceiling

The standard drug-blind metric, global Pearson  $r$  over all test pairs, conflates two signals: between-drug potency ranking and within-drug cell sensitivity ranking<sup>5</sup>. A drug-mean oracle that predicts each compound’s average  $IC_{50}$  regardless of cell line already surpasses the reported drug-blind ceiling by a wide margin (global  $r = 0.837$  vs. the published ceiling of  $\sim 0.51$ ), demonstrating that the ceiling reflects failure to predict drug potency for unseen compounds, not failure to rank cells.

Global  $r$  decomposes into a weighted sum of between-drug and within-drug components (Supplementary Note 1). In GDSC2, between-drug variance dominates because drug means span an order of magnitude more than within-drug variation, so global  $r$  is driven almost entirely by scale prediction (Fig. 2a).

Per-drug Pearson  $r$ , the correlation within each test drug across cell lines averaged over drugs, isolates cell ranking. Training with per-drug  $z$ -scored targets collapsed global  $r$  while preserving per-drug  $r$ , confirming that the two signals are independent (Fig. 2a). Cell-blind CV on held-out cell lines inverts the conventional ranking: familiar cells enable accurate ranking without drug information, but unfamiliar cells cannot be ranked even when the drug is known (Fig. 2d).

Cross-assay replicate concordance between GDSC1 and GDSC2 provides an empirical ceiling of  $r = 0.754$  (9 anchor drugs, per-drug range 0.57–0.93). The zero-shot baseline already reaches 86% of this ceiling (Fig. 2d).

### Evaluation artifacts in three prominent models

PASO<sup>14</sup> reported drug-blind  $r = 0.745$ . Examination of the publicly available implementation revealed checkpoint selection by maximizing *test-set* Pearson  $r$  each epoch with no validation holdout. DeepCDR<sup>15</sup> and DrugCell<sup>16</sup> showed the same pattern. Under a fair protocol with a validation holdout, test-set leakage and best-fold selection together account for the gap between the fair mean and the published figure (Extended Data Fig. 1). Leakage was confirmed in 23 of

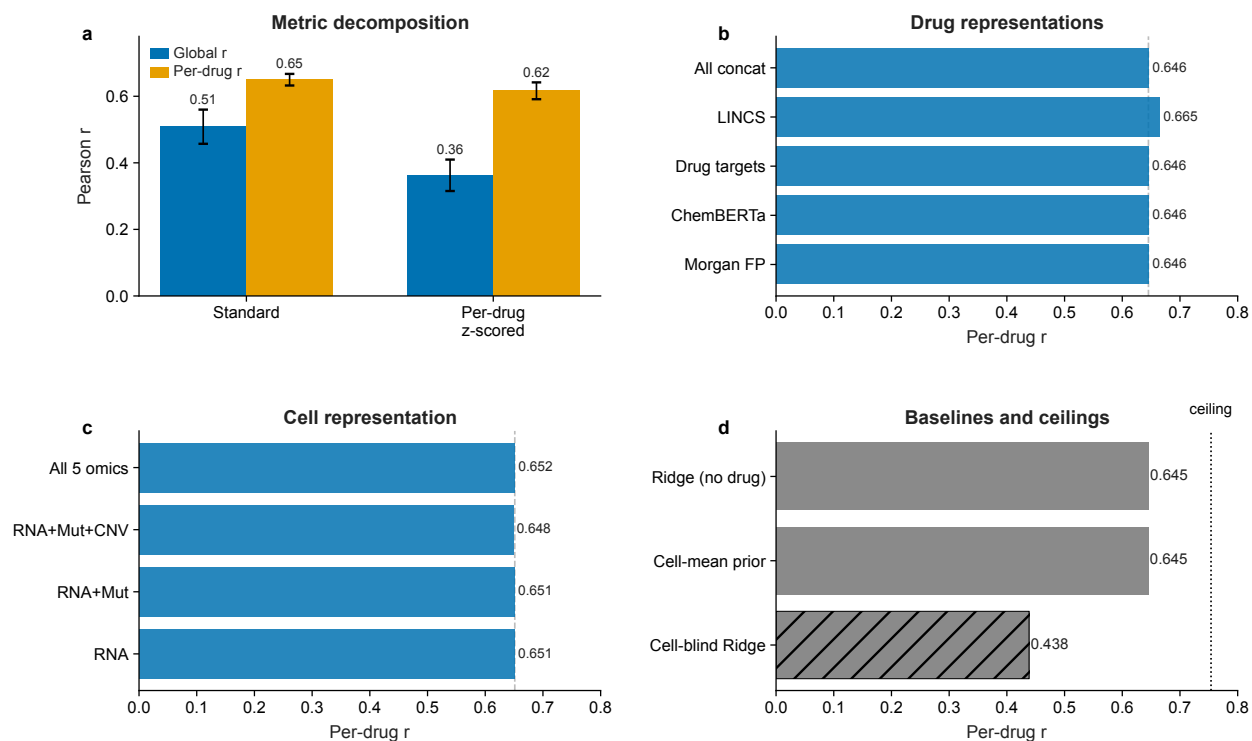


**Fig. 2 — Per-drug  $r$  reveals a ceiling invisible to global  $r$ , and no drug representation improves within-drug cell ranking.** **a**, Global vs. per-drug  $r$  under standard training and  $z$ -scoring. **b**, Per-drug  $r$  across drug feature types (structural and functional), all within  $\Delta \leq +0.001$  of the no-drug-features baseline (dashed). LINCS is evaluated on its 104-drug covered subset (within-subset  $\Delta = +0.001$ ). **c**, Omics ablation. RNA-seq alone achieves per-drug  $r = 0.651$ ; mutations and further modalities each add  $\leq +0.001$ . **d**, Per-drug  $r$  for three reference predictors: cell-blind ridge (out-of-distribution cells), cell-mean prior ( $K = 0$  zero-shot), and ridge without drug features (drug-blind standard). Dotted line: within-assay replicate ceiling ( $r = 0.754$ ).

32 audited methods across the field<sup>13</sup>. We therefore ask, under a corrected evaluation protocol, whether any drug encoding can improve per-drug  $r$ .

### Drug representations do not improve within-drug ranking

We evaluated all major drug representation types under ridge regression with 10-fold drug-blind CV on PASO splits. No encoding improved per-drug  $r$  beyond  $\Delta = +0.001$  of the cell-only baseline (Fig. 2b, Extended Data Table 1). This null held for Morgan fingerprints, ChemBERTa embeddings, drug-target vectors, and LINCS L1000 perturbation signatures<sup>9</sup>. The LINCS result is particularly informative because these signatures encode a drug’s transcriptional effect rather than its chemical structure, ruling out the hypothesis that structural representations fail because they lack mechanistic content. The null also held under scaffold-stratified splits ( $\Delta = +0.001$ ).

An 11.7M-parameter Transformer encoder replicated the null under the same protocol. Morgan fingerprints gave  $\Delta = +0.008$ , and LINCS and drug-target vectors gave no significant improvement. An omics ablation confirmed that RNA-seq alone captures nearly all predictive signal, with mutations and further modalities adding negligibly (Fig. 2c). Cell-representation expressiveness is not the bottleneck.

The null replicated across three independent datasets (CTRPv2, BeatAML, and PRISM, Extended Data Table 3). On PRISM, the effect was marginal, consistent with its pharmacologically diverse viability-based assay. The uniformity of the null across all encoding types shifts the question from representation quality to training distribution. Does MoA information fail because it cannot be encoded, or because the training distribution is misaligned?

### Training distribution alignment outperforms drug encoding

If models transfer within but not across MoA classes<sup>10</sup>, is the failure *representational*, reflecting missing MoA knowledge, or *distributional*, reflecting MoA-mismatched training examples? We dissected this by channeling the same MoA information through two routes: as a drug feature (a 24-class one-hot label concatenated with cell features) or as a training distribution constraint ( $20\times$  upweighting of same-MoA samples, or within-MoA leave-one-out CV).

Under ridge regression, supplying MoA as a feature left per-drug  $r$  unchanged while increasing global  $r$  by +0.041 (Fig. 3a, Extended Data Table 2). The global  $r$  gain is expected because a

drug-constant label shifts predicted means without altering relative cell sensitivities. In contrast,  $20\times$  upweighting of same-MoA training samples produced large gains for targeted kinase inhibitors, raising ERK MAPK and EGFR per-drug  $r$  well above their all-drug baselines (Extended Data Table 2). The same information produces qualitatively different outcomes depending on whether it enters through representation or distribution.

The Transformer partially overcomes this limitation. MoA one-hot gave a marginally significant gain (one-sided Wilcoxon  $P = 0.053$ ) that was abolished by a permuted-label control ( $P = 0.014$  for the real-vs.-permuted difference), confirming that the Transformer exploits class identity rather than dimensionality reduction (Fig. 3a). Yet this representational gain remains an order of magnitude smaller than the within-MoA training gains for targeted classes. Distribution alignment is the primary mechanism.

Within-MoA leave-one-out produced the largest gains. ERK MAPK per-drug  $r$  rose from 0.427 to 0.723 across 11 drugs, and EGFR from 0.425 to 0.799 across 7 drugs. Both values exceed the within-class profile concordances, indicating that supervised models extract a generalizable mapping beyond nearest-drug transfer (Fig. 3b).

The improvement was class-specific and graded by pathway specificity. PI3K/MTOR and RTK signaling showed smaller but positive gains, as expected for pharmacologically heterogeneous classes (Supplementary Table 4). Apoptosis regulation showed no improvement, a genuine biological limit attributable to within-class mechanistic heterogeneity. Cell-division classes were unaffected because all-drug training already captures the pan-cancer fragility signal for these pathways. CTRPv2 replication confirmed the EGFR pattern ( $\Delta = +0.371$  for 8 EGFR inhibitors).

Pan-cancer training creates a dominant cell-fragility signal that suppresses the weaker, pathway-specific signals governing targeted kinase inhibitor response. The upweighting result supports this interpretation: gains emerge even when all training drugs are retained, ruling out the alternative that within-MoA training simply presents an easier problem with fewer samples. Consistent with this mechanism, the signals recovered by within-MoA training correspond to known oncogenic drivers<sup>17,18</sup>. *EGFR*-mutant cell lines are significantly more sensitive to all EGFR inhibitors tested (Fig. 4a), and *BRAF/KRAS*-mutant cell lines show large sensitivity differences to ERK MAPK inhibitors (Cohen’s  $d > 0.8$ , Fig. 4b). Pan-cancer co-training dilutes these mutation-stratified signals because most training drugs target different oncogenic pathways.

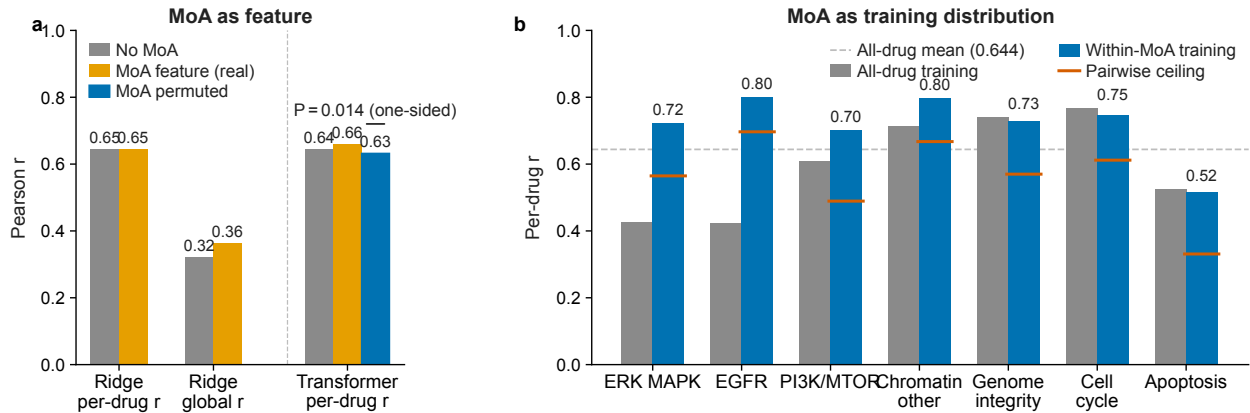


**Fig. 3 — Training distribution determines the prediction ceiling for targeted kinase inhibitors. Drug encoding does not.** **a**, MoA identity as a drug feature. Ridge global  $r$  rises by +0.041; ridge per-drug  $r$  is unchanged. The Transformer’s marginal gain with real labels is abolished by label permutation (one-sided Wilcoxon  $P = 0.014$ ). **b**, MoA identity as a training distribution. Per-drug  $r$  for seven MoA classes under all-drug (gray) vs. within-MoA (blue) training. Orange lines, pairwise profile concordance (nearest-neighbor transfer baseline).

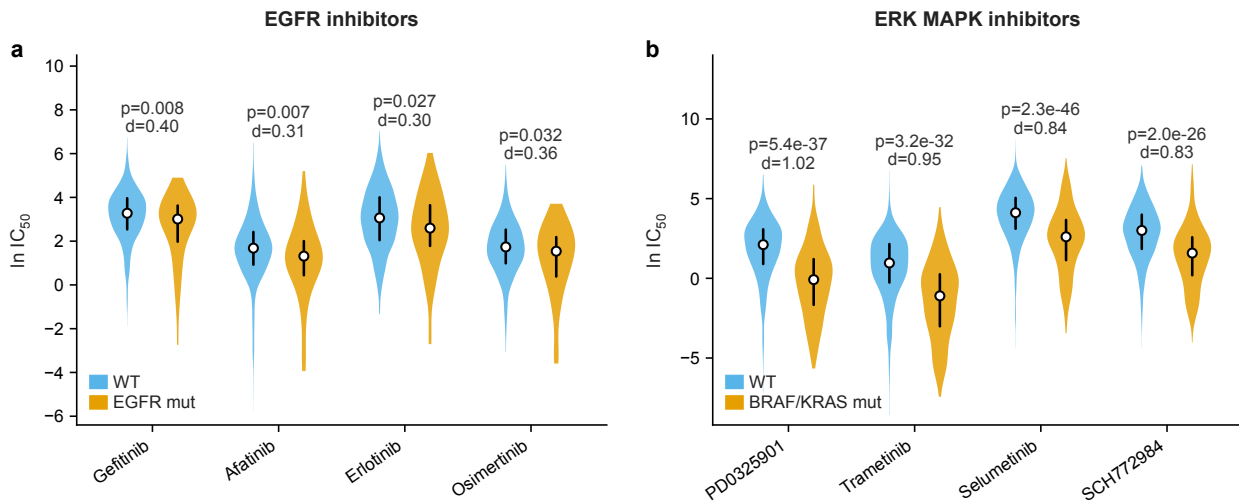


**Fig. 4 — Oncogenic driver mutations stratify sensitivity to matched inhibitors.** **a**,  $\ln IC_{50}$  distributions for four EGFR inhibitors in *EGFR*-mutant ( $n = 60$ , orange) vs. wild-type (blue) cell lines. Mutant cells are significantly more sensitive (one-sided Mann–Whitney  $P < 0.05$ , Cohen’s  $d = 0.30$ – $0.40$ ). **b**,  $\ln IC_{50}$  for four ERK MAPK inhibitors in *BRAF/KRAS*-mutant ( $n \geq 227$  per drug, orange) vs. wild-type (blue) cell lines. Mutant cells are substantially more sensitive (Cohen’s  $d = 0.83$ – $1.02$ ,  $P < 10^{-25}$ ).

## Response profile matching improves within-drug ranking

MoA-stratified training requires knowing the drug class in advance. We next ask whether pilot  $IC_{50}$  observations of the test drug, which require no class information, can close the gap independently.

Given  $K$   $IC_{50}$  observations for a new drug, response profile matching identifies training drugs with similar response patterns on the observed cells and transfers their sensitivity profiles. At low  $K$ , too few observations yield unreliable matches and the blended estimator defaults to the cell-mean prior. Above approximately 20 observations, correlation estimates stabilize and matching adds genuine value, reaching per-drug  $r = 0.701$  at  $K = 50$  (Fig. 5). A permuted-drug control confirmed that incorrect pairing actively degrades performance, falling below the cell-mean prior.

MoA-stratified training and response matching trade different resources. Within-MoA training requires the drug class label and a same-class training set, whereas response matching requires only pilot observations of the test drug itself. For EGFR, combining the two at  $K = 20$  matched within-MoA training alone. For ERK MAPK, response matching alone at  $K = 50$  exceeded within-MoA training without requiring class information. Direct observations of the test drug encode its specific response profile more precisely than proxy training on related drugs, and the advantage grows with the number of pilot observations.

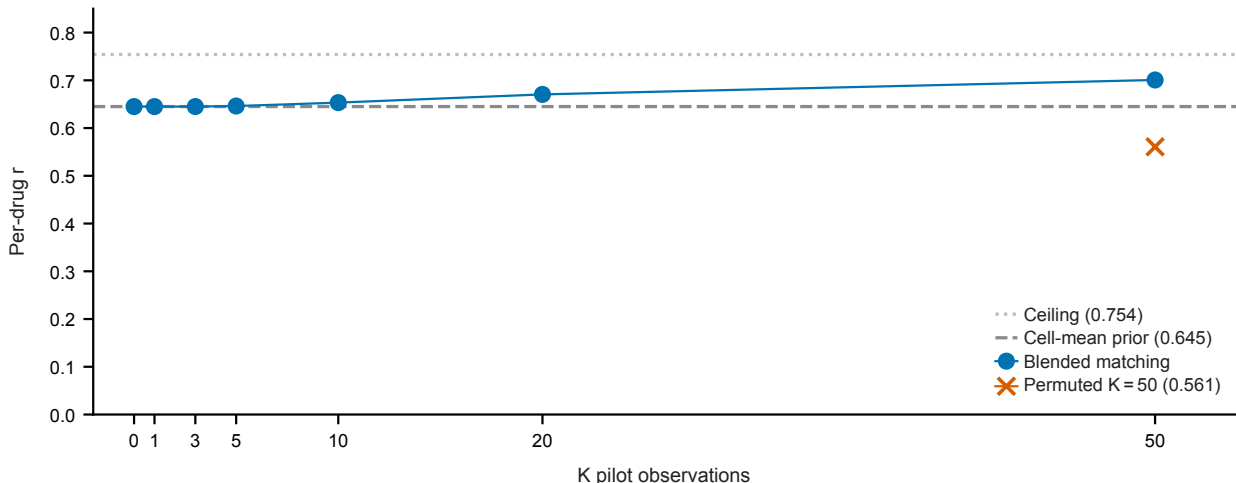


**Fig. 5 — Pilot profiling consistently improves within-drug cell ranking above  $K = 10$  observations.** Per-drug  $r$  vs.  $K$  pilot observations on GDSC2. The cell-mean prior ( $K = 0$ , dashed) achieves  $r = 0.645$  without any drug-specific information. Blended matching exceeds this at  $K \geq 20$  and reaches  $r = 0.701$  at  $K = 50$ , against a replicate-pair ceiling of 0.754. A permuted  $K = 50$  control (cross) confirms the gain requires correct cell–drug pairing, not response-scale alignment.

Response matching generalizes across independent datasets (Fig. 6). On CTRPv2, 812 Broad cell lines absent from GDSC2 training identify informative matches through shared omics features. On patient-derived BeatAML<sup>19</sup>, per-drug  $r$  rises from 0.453 to 0.521 at  $K = 50$ , confirming transfer to *ex vivo* patient samples. PRISM’s  $K$ -curve collapses because its pharmacologically diverse repurposing library lacks functional analogs among GDSC2’s targeted/cytotoxic training drugs, defining the practical boundary of the approach (Fig. 6c).

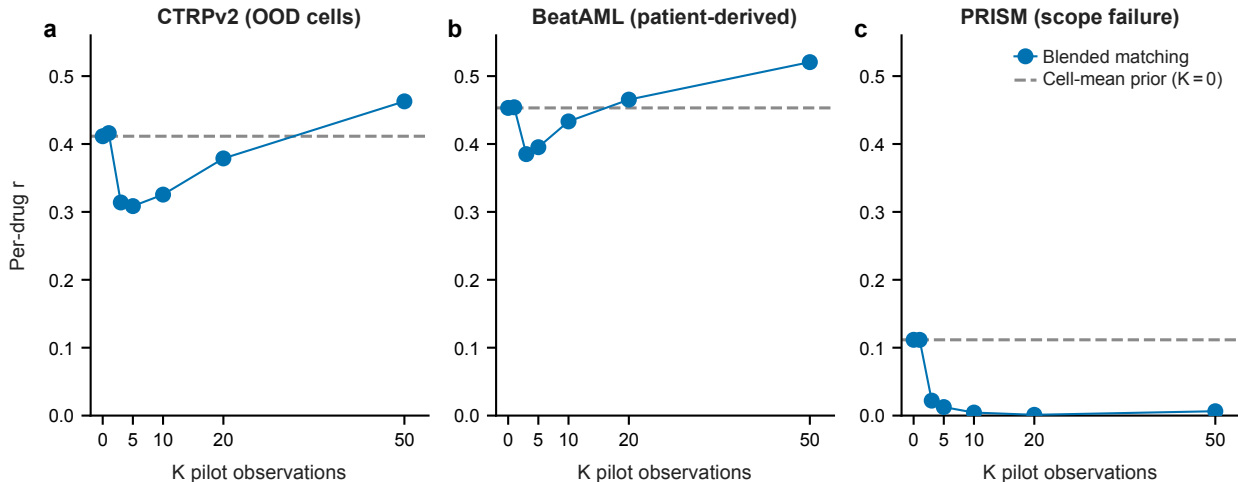


**Fig. 6** — Response matching generalizes across independent cell lines and patient-derived samples but requires functional drug analogs in the training set. **a**, CTRPv2 (out-of-distribution cells). Per-drug  $r$  rises by +0.051 at  $K = 50$  using 812 Broad cell lines absent from GDSC2 training. **b**, BeatAML (patient-derived). Per-drug  $r$  rises from 0.453 to 0.521 at  $K = 50$  across 520 AML patients. **c**, PRISM (scope failure). The  $K$ -curve collapses at  $K \geq 3$  because PRISM’s repurposing library lacks functional analogs among GDSC2’s training drugs. Transient dip at  $K = 3$ –10 in panels a and b reflects unreliable estimates from too few observations. Cell-mean prior (dashed line) is the  $K = 0$  reference in each panel.

## Discussion

The assumption that improved drug representations would raise drug-blind prediction ceilings has driven a decade of encoder development in cancer pharmacogenomics. Our results redefine the constraint. The bottleneck is distributional, not representational. Mechanistically heterogeneous co-training suppresses the pathway-specific signals that any encoder would transmit regardless of its expressiveness, and restructuring the training distribution removes this suppression directly. Independent work has converged on the same null in drug-blind evaluation<sup>10,11</sup> and in the drug-seen

regime<sup>12</sup>, indicating that encoder development has been addressing the wrong variable.

The mechanism traces to training distribution heterogeneity. Co-training on mechanistically diverse drugs forces the model to learn a response map averaged across MoAs. Pathway-specific cell features that predict sensitivity for EGFR inhibitors conflict with those for topoisomerase inhibitors, and the model resolves this conflict by learning features predictive only of mean potency. A drug encoder, regardless of its expressiveness, feeds into a model whose response map has been smoothed across all MoAs. LINCS L1000 signatures capture a drug’s average transcriptional effect on a reference population, not cell-specific response variation. Drug-target vectors are too coarse to resolve the pathway context differences that distinguish sensitive from resistant cell lines. The sole partial exception, MoA categorical identity in the Transformer, was abolished by label permutation, confirming that the residual signal reflects implicit class-conditional partitioning of the training distribution rather than representational content.

Within-MoA training distinguishes artifactual ceilings from genuine biological limits. Aligned training exceeded within-class profile concordances for ERK MAPK and EGFR, indicating that supervised models extract a generalizable mapping beyond profile similarity. Classes with high within-class mechanistic heterogeneity, such as Apoptosis regulation, are not addressable by distribution alignment alone because the training drugs within the class do not share a coherent response pattern to transfer. Response matching provides a complementary route, generalizing to patient-derived data (BeatAML) and to cell lines absent from training (CTRPv2), but requiring functional drug analogs in the reference set.

Checkpoint selection artifacts explain a substantial portion of reported progress as methodological inflation, consistent with the 72% leakage rate documented across the field<sup>13</sup>. Per-drug  $r$ , the cell-mean prior as a free baseline, and replicate concordance as a ceiling give the field evaluation tools to separate genuine advances from metric optimization.

Both approaches have scope conditions. Response matching requires functional drug analogs in the reference set, and within-MoA training requires mechanistically coherent drug classes with strong pathway dependence. Beyond these scope conditions, all results rest on cell-line  $IC_{50}$  values, which abstract away *in vivo* pharmacokinetics, tumor microenvironment effects, clonal heterogeneity, and drug combinations. Whether distribution alignment translates to improved patient response requires prospective validation in clinical cohorts.

The representation–distribution dissociation may extend beyond cancer pharmacogenomics. Any co-training distribution with mechanistic heterogeneity can suppress signals relevant to a specific test condition. Benchmarking should evaluate training distribution alongside representation quality to distinguish improved encoding from improved data curation.

## Methods

### Data

We used GDSC2<sup>20</sup> (233 drugs with valid Morgan fingerprints, 687 cancer cell lines with matched RNA and mutation profiles) with RNA-seq gene expression (19,193 protein-coding genes) and somatic mutation profiles (12,301 genes) from the Cancer Cell Line Encyclopedia<sup>21</sup>. The response variable was  $\ln(\text{IC}_{50})$  in  $\mu\text{M}$ . For LINCS experiments, Harmonizome<sup>22</sup> consensus perturbation profiles (104 GDSC2 drugs matched by name) were PCA-reduced to 64 dimensions. Cross-dataset validation used CTRPv2<sup>23</sup> (545 compounds, 812 cell lines, AUC, 66 drugs overlapping GDSC2), BeatAML<sup>19</sup> (155 drugs, 520 patients, *ex vivo* AUC, drugs with  $\geq 20$  patients), and PRISM Repurposing<sup>24</sup> (1,079 drugs).

### Evaluation

All experiments used  $k$ -fold drug-blind CV (default  $k = 5$ ,  $k = 10$  for PASO splits). For ridge regression, the test fold was held out and the remaining  $k - 1$  folds were used for training. No validation fold is required. For the Transformer encoder, 10% of training drugs in each fold were held out as a drug-blind validation set for epoch selection, with the remaining  $\sim 90\%$  used for training. The test fold was evaluated once after model selection. We report global Pearson  $r$  (across all test pairs) and per-drug Pearson  $r$  (correlation within each test drug across cell lines with  $\geq 5$  observations, averaged over drugs). Per-drug  $r$  is invariant to additive and multiplicative per-drug transformations of the target.

### Models

The primary model was ridge regression ( $\alpha = 1.0$ ) with RNA PCA-550 + mutation PCA-200 cell features, with drug features appended when specified.

A Transformer encoder<sup>25</sup> was used for representation ablation experiments. The architecture consists of 4 pre-norm layers (LayerNorm before attention and feedforward), 256-dim hidden size, 8 attention heads, feedforward dimension 1024. Each input modality is projected to 256 dimensions (RNA:  $\text{Linear}(n_{\text{genes}} \rightarrow 256)$ , mutations:  $\text{Linear}(n_{\text{mut}} \rightarrow 256)$ , drug:  $\text{Linear}(d_{\text{drug}} \rightarrow 256)$ ) and summed with a learnable modality-type embedding before self-attention across the three tokens. During training, each omics token is independently zeroed with probability 0.3 (modality dropout). The prediction head mean-pools token outputs, applies LayerNorm, and maps to a scalar ( $\text{Linear}(256, 1)$ ). Total parameters: 11.7M (dominated by the RNA projection). Training used AdamW (lr =  $10^{-3}$ , weight decay  $10^{-4}$ , cosine schedule,  $\eta_{\text{min}} = 10^{-5}$ , with 10-epoch linear warmup), gradient clipping at max norm 1.0, 200 epochs, batch size 256. Drug feature dimensions tested were Morgan FP (2048), LINCS PCA-64, drug-target PCA-256, MoA one-hot (24), and zero-vector (no-drug baseline).

### Permuted-MoA control

To distinguish class-identity information from dimensionality-reduction effects, we constructed a permuted-MoA condition by randomly shuffling drug-to-pathway assignments across all drugs (fixed seed 42) while preserving class-size distribution. The same 10-fold protocol was applied. If the MoA gain reflects class identity, permuted labels should perform at or below the no-drug baseline.

### Response profile matching

Response profile matching extends the collaborative filtering principle<sup>26,27</sup> to the drug-blind cold-start setting. Given  $K$  observed  $\text{IC}_{50}$  values for a new drug, we compute Pearson  $r$  between the  $K$ -cell response vector and each training drug’s response on the same cells, select the top  $N = 5$  training drugs by correlation magnitude, and predict remaining cells as a weighted average of selected training drug profiles, with negative correlations zero-weighted. The blended estimator uses a CV-optimal convex combination of the cell-mean prior and the matched prediction. The blend weight  $w$ , selected by inner CV per fold, dominates the  $K$ -dependent sensitivity. At small  $K$  the weight collapses to the prior. No model training is required.

## MoA-stratified training

Three conditions. *MoA one-hot*: an  $n_{\text{MoA}}$ -dimensional one-hot vector (GDSC2 Target Pathway, 24 classes) concatenated with cell features in all-drug CV. *MoA-weighted*: all-drug training with same-MoA samples weighted  $20\times$  relative to other drugs (weight selected by grid search over  $\{1, 2, 5, 10, 20\}$  on validation folds). *Within-MoA CV*: leave-one-drug-out using only same-MoA training drugs, with RNA PCA-550 + mutation PCA-200 features fitted on all training cell lines, ridge ( $\alpha = 1.0$ ), mean and s.d. reported over drugs within each class.

## PASO reproduction

PASO’s published 10-fold split files were used. PASO-style evaluation retained the checkpoint maximizing test-set Pearson  $r$  per epoch (200 epochs, no validation holdout). Fair evaluation held out 10% of training data as a validation set and selected the checkpoint maximizing validation  $r$ . The test fold was evaluated once.

## Statistical analysis

Pearson correlations were computed on held-out test folds only. Per-drug  $r$  is reported as mean  $\pm$  s.d. across drugs. Condition differences were assessed by paired Wilcoxon signed-rank test (two-sided unless stated otherwise).  $P$  values are exact where sample size permits. Effect sizes are absolute  $\Delta r$ . Seed sensitivity was assessed over 10 random fold assignments. No multiple-testing correction was applied to exploratory secondary analyses (MoA class comparisons beyond ERK MAPK and EGFR, omics ablation variants). Confirmatory analyses (drug representation null, MoA feature vs. distribution dissociation) used pre-specified primary comparisons.

Biomarker associations used binary non-synonymous mutation status from DepMap 24Q4 somatic mutation calls (synonymous variants excluded). Group comparisons (mutant vs. wild-type) used a one-sided Mann–Whitney U test with the alternative hypothesis that mutant  $\text{IC}_{50} < \text{wild-type}$ , and pooled Cohen’s  $d$  as effect size.

## Computational protocol

The headline drug representation ablation and MoA experiments used 10-fold drug-blind CV with 200 epochs (Transformer encoder) or no iterative training (ridge). Exploratory Transformer-encoder ablations (drug feature real/random/zero and PRISM) used reduced configurations (3–5 folds, 15–50 epochs) for computational efficiency. All headline numbers reported in the main text use the full protocol. ChemBERTa<sup>8</sup> pre-trained SMILES embeddings (768-dim) were evaluated at raw dimensionality and PCA-reduced to 64 and 128 dimensions. For scaffold-stratified evaluation, drugs were partitioned into 5 folds using Bemis–Murcko scaffold clustering<sup>28</sup> (219 unique scaffolds). All experiments were run on an NVIDIA DGX Spark workstation. Ridge regression completed in under one minute per fold, Transformer training in approximately 2 hours per 10-fold run.

## Code availability

All source code is available at <https://github.com/TaekyungHeo/drug-response-distribution>.

## References

- [1] James C. Costello, Laura M. Heiser, Elisabeth Georgii, Mehmet Gönen, Michael P. Menden, Nicholas J. Wang, Mukesh Bansal, Muhammad Ammad-ud din, Petteri Hintsanen, Suleiman A. Khan, John-Patrick Mpindi, Olli Kallioniemi, Antti Honkela, Tero Aittokallio, Krister Wennerberg, James J. Collins, Dan Gallahan, Dinah Singer, Julio Saez-Rodriguez, Samuel Kaski, Joe W. Gray, and Gustavo Stolovitzky. A community effort to assess and improve drug sensitivity prediction algorithms. *Nat. Biotechnol.*, 32:1202–1212, 2014. doi: 10.1038/nbt.2877.
- [2] George Adam, Ladislav Rampásek, Zhaleh Safikhani, Petr Smirnov, Benjamin Haibe-Kains, and Anna Goldenberg. Machine learning approaches to drug response prediction: challenges and recent progress. *npj Precis. Oncol.*, 4:19, 2020. doi: 10.1038/s41698-020-0122-1.
- [3] Yiheng Zhu, Zhenqiu Ouyang, Wenbo Chen, Ruiwei Feng, Danny Z. Chen, Ji Cao, and Jian Wu. TGSA: protein–protein association-based twin graph neural networks for drug response prediction with similarity augmentation. *Bioinformatics*, 38:461–468, 2022. doi: 10.1093/bioinformatics/btab650.

- [4] Yewon Han, Sunghyun Kim, Eunyi Jeong, Sungkyung Lee, Seokwoo Yun, and Sangsoo Lim. DiSPA: differential substructure-pathway attention for drug response prediction. *Preprint at arXiv*, 2026. arXiv:2601.14346.
- [5] Francesco Codicè, Corrado Pancotti, Cesare Rollo, Yves Moreau, Piero Fariselli, and Daniele Raimondi. The specification game: rethinking the evaluation of drug response prediction for precision oncology. *J. Cheminform.*, 17:33, 2025. doi: 10.1186/s13321-025-00972-y.
- [6] Nikhil Branson, Pedro R. Cutillas, and Conrad Bessant. Understanding the sources of performance in deep drug response models reveals insights and improvements. *Bioinformatics*, 41: i142–i149, 2025. doi: 10.1093/bioinformatics/btaf255.
- [7] David Rogers and Mathew Hahn. Extended-connectivity fingerprints. *J. Chem. Inf. Model.*, 50:742–754, 2010. doi: 10.1021/ci100050t.
- [8] Seyone Chithrananda, Gabriel Grand, and Bharath Ramsundar. ChemBERTa: large-scale self-supervised pretraining for molecular property prediction. *Preprint at arXiv*, 2020. arXiv:2010.09885.
- [9] Aravind Subramanian, Rajiv Narayan, Steven M. Corsello, David D. Peck, Ted E. Natoli, Xiaodong Lu, Joshua Gould, John F. Davis, Andrew A. Tubelli, Jacob K. Asiedu, David L. Lahr, Jodi E. Hirschman, Zihan Liu, Melanie Donahue, Bina Julian, Mariya Khan, David Wadden, Ian C. Smith, Daniel Lam, Arthur Liberzon, Courtney Toder, Mukta Bagul, Marek Orzechowski, Oana M. Enache, Federica Piccioni, Sarah A. Johnson, Nicholas J. Lyons, Alice H. Berger, Alykhan F. Shamji, Angela N. Brooks, Anita Vrcic, Corey Flynn, Jacqueline Rosains, David Y. Takeda, Roger Hu, Desiree Davison, Justin Lamb, Kristin Ardlie, Larson Hogstrom, Peyton Greenside, Nathanael S. Gray, Paul A. Clemons, Serena Silver, Xiaoyun Wu, Wen-Ning Zhao, Willis Read-Button, Xiaohua Wu, Stephen J. Haggarty, Lucienne V. Ronco, Jesse S. Boehm, Stuart L. Schreiber, John G. Doench, Joshua A. Bittker, David E. Root, Bang Wong, and Todd R. Golub. A next generation connectivity map: L1000 platform and the first 1,000,000 profiles. *Cell*, 171:1437–1452.e17, 2017. doi: 10.1016/j.cell.2017.10.049.
- [10] William G. Herbert, Nicholas Chia, Paul A. Jensen, and Marina R. S. Walther-Antonio.

- Monotherapy cancer drug-blind response prediction is limited to intraclass generalization. *PLoS Comput. Biol.*, 22:e1013232, 2026. doi: 10.1371/journal.pcbi.1013232.
- [11] Judith Bernett, Pascal Iversen, Mario Picciani, Mathias Wilhelm, Katharina Baum, and Markus List. From hype to health check: critical evaluation of drug response prediction models with DrEval. *Preprint at bioRxiv*, 2025. doi: 10.1101/2025.05.26.655288.
- [12] Francesco Carli, Pierluigi Di Chiaro, Mariangela Morelli, Chakit Arora, Luisa Bisceglia, Natalia De Oliveira Rosa, Alice Cortesi, Sara Franceschi, Francesca Lessi, Anna Luisa Di Stefano, Orazio Santo Santonocito, Francesco Pasqualetti, Paolo Aretini, Pasquale Miglionico, Giuseppe R. Diaferia, Fosca Giannotti, Pietro Liò, Miquel Duran-Frigola, Chiara Maria Mazzanti, Gioacchino Natoli, and Francesco Raimondi. Learning and actioning general principles of cancer cell drug sensitivity. *Nat. Commun.*, 16:1654, 2025. doi: 10.1038/s41467-025-56827-5.
- [13] Amir Asiaee, Jared Strauch, Leila Azinfar, Samhita Pal, Heather H. Pua, James P. Long, and Kevin R. Coombes. Widespread data leakage inflates accuracy and corrupts biomarker discovery in cancer drug response prediction. *Preprint at bioRxiv*, 2026. doi: 10.64898/2026.02.05.704016.
- [14] Yang Wu, Ming Chen, and Yufang Qin. Anticancer drug response prediction integrating multi-omics pathway-based difference features and multiple deep learning techniques. *PLoS Comput. Biol.*, 21:e1012905, 2025. doi: 10.1371/journal.pcbi.1012905.
- [15] Qiao Liu, Zhiqiang Hu, Rui Jiang, and Mu Zhou. DeepCDR: a hybrid graph convolutional network for predicting cancer drug response. *Bioinformatics*, 36:i911–i918, 2020. doi: 10.1093/bioinformatics/btaa822.
- [16] Brent M. Kuenzi, Jisoo Park, Samson H. Fong, Kyle S. Sanchez, John Lee, Jason F. Kreisberg, Jianzhu Ma, and Trey Ideker. Predicting drug response and synergy using a deep learning model of human cancer cells. *Cancer Cell*, 38:672–684.e6, 2020. doi: 10.1016/j.ccell.2020.09.014.
- [17] Thomas J. Lynch, Daphne W. Bell, Raffaella Sordella, Sarada Gurubhagavatula, Ross A. Okimoto, Brian W. Brannigan, Patricia L. Harris, Sara M. Haserlat, Jeffrey G. Supko, Frank G. Haluska, David N. Louis, David C. Christiani, Jeff Settleman, and Daniel A. Haber. Activating

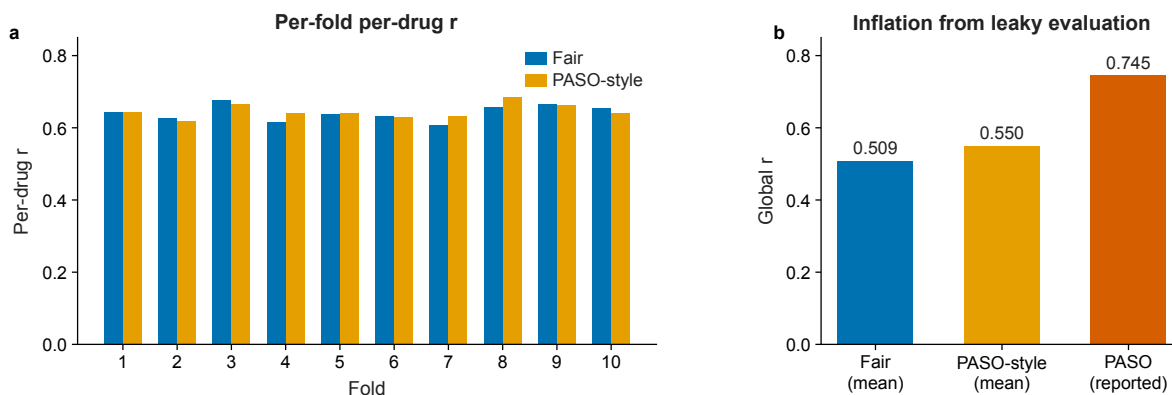
- mutations in the epidermal growth factor receptor underlying responsiveness of non-small-cell lung cancer to gefitinib. *N. Engl. J. Med.*, 350:2129–2139, 2004. doi: 10.1056/nejmoa040938.
- [18] Helen Davies, Graham R. Bignell, Charles Cox, Philip Stephens, Sarah Edkins, Sheila Clegg, Jon Teague, Hayley Woffendin, Mathew J. Garnett, William Bottomley, Neil Davis, Ed Dicks, Rebecca Ewing, Yvonne Floyd, Kristian Gray, Sarah Hall, Rachel Hawes, Jaime Hughes, Vivian Kosmidou, Andrew Menzies, Catherine Mould, Adrian Parker, Claire Stevens, Stephen Watt, Steven Hooper, Rebecca Wilson, Hiran Jayatilake, Barry A. Gusterson, Colin Cooper, Janet Shipley, Darren Hargrave, Katherine Pritchard-Jones, Norman Maitland, Georgia Chenevix-Trench, Gregory J. Riggins, Darell D. Bigner, Giuseppe Palmieri, Antonio Cossu, Adrienne Flanagan, Andrew Nicholson, Judy W. C. Ho, Suet Y. Leung, Siu T. Yuen, Barbara L. Weber, Hilliard F. Seigler, Timothy L. Darrow, Hugh Paterson, Richard Marais, Christopher J. Marshall, Richard Wooster, Michael R. Stratton, and P. Andrew Futreal. Mutations of the BRAF gene in human cancer. *Nature*, 417:949–954, 2002. doi: 10.1038/nature00766.
- [19] Daniel Bottomly, Nicola Long, Anna Reister Schultz, Stephen E. Kurtz, Cristina E. Tognon, Kara Johnson, Melissa Abel, Anupriya Agarwal, Sammantha Avaylon, Erik Benton, Aurora Blucher, Uma Borate, Theodore P. Braun, Jordana Brown, Jade Bryant, Russell Burke, Amy Carlos, Bill H. Chang, Hyun Jun Cho, Stephen Christy, Cody Coblentz, Aaron M. Cohen, Amanda d’Almeida, Rachel Cook, Alexey Danilov, Kim-Hien T. Dao, Michie Degnin, James Dibb, Christopher A. Eide, Isabel English, Stuart Hagler, Heath Harrelson, Rachel Henson, Hiberny Ho, Sunil K. Joshi, Brian Junio, Andy Kaempf, Yoko Kosaka, Ted Laderas, Matt Lawhead, Hyunjung Lee, Jessica T. Leonard, Chenwei Lin, Evan F. Lind, Selina Qiuying Liu, Pierrette Lo, Marc M. Loriaux, Samuel Luty, Julia E. Maxson, Tara Macey, Jacqueline Martinez, Jessica Minnier, Andrea Montebianco, Motomi Mori, Quinlan Morrow, Dylan Nelson, Justin Ramsdill, Angela Rofelty, Alexandra Rogers, Kyle A. Romine, Peter Ryabinin, Jennifer N. Saultz, David A. Sampson, Samantha L. Savage, Robert Schuff, Robert Searles, Rebecca L. Smith, Stephen E. Spurgeon, Tyler Sweeney, Ronan T. Swords, Aashis Thapa, Karina Thiel-Klare, Elie Traer, Jake Wagner, Beth Wilmot, Joelle Wolf, Guanming Wu, Amy Yates, Haijiao Zhang, Christopher R. Cogle, Robert H. Collins, Michael W. Deininger, Christopher S. Hourigan, Craig T. Jordan, Tara L. Lin, Micaela E. Martinez, Rachel R. Pallapati, Daniel A. Pollyea,

- Anthony D. Pomicter, Justin M. Watts, Scott J. Weir, Brian J. Druker, Shannon K. McWeeney, and Jeffrey W. Tyner. Integrative analysis of drug response and clinical outcome in acute myeloid leukemia. *Cancer Cell*, 40:850–864.e9, 2022. doi: 10.1016/j.ccell.2022.07.002.
- [20] Francesco Iorio, Theo A. Knijnenburg, Daniel J. Vis, Graham R. Bignell, Michael P. Menden, Michael Schubert, Nanne Aben, Emanuel Gonçalves, Syd Barthorpe, Howard Lightfoot, Thomas Cokelaer, Patricia Greninger, Ewald van Dyk, Han Chang, Heshani de Silva, Holger Heyn, Xianming Deng, Regina K. Egan, Qingsong Liu, Tatiana Mironenko, Xenia Mitropoulos, Laura Richardson, Jinhua Wang, Tinghu Zhang, Sebastian Moran, Sergi Sayols, Maryam Soleimani, David Tamborero, Nuria Lopez-Bigas, Petra Ross-Macdonald, Manel Esteller, Nathanael S. Gray, Daniel A. Haber, Michael R. Stratton, Cyril H. Benes, Lodewyk F. A. Wessels, Julio Saez-Rodriguez, Ultan McDermott, and Mathew J. Garnett. A landscape of pharmacogenomic interactions in cancer. *Cell*, 166:740–754, 2016. doi: 10.1016/j.cell.2016.06.017.
- [21] Mahmoud Ghandi, Franklin W. Huang, Judit Jané-Valbuena, Gregory V. Kryukov, Christopher C. Lo, E. Robert McDonald III, Jordi Barretina, Ellen T. Gelfand, Craig M. Bielski, Haoxin Li, Kevin Hu, Alexander Y. Andreev-Drakhlin, Jaegil Kim, Julian M. Hess, Brian J. Haas, François Aguet, Barbara A. Weir, Michael V. Rothberg, Brenton R. Paoella, Michael S. Lawrence, Rehan Akbani, Yiling Lu, Hong L. Tiv, Prafulla C. Gokhale, Antoine de Weck, Ali Amin Mansour, Coyin Oh, Juliann Shih, Kevin Hadi, Yanay Rosen, Jonathan Bistline, Kavitha Venkatesan, Anupama Reddy, Dmitriy Sonkin, Manway Liu, Joseph Lehar, Joshua M. Korn, Dale A. Porter, Michael D. Jones, Javad Golji, Giordano Caponigro, Jordan E. Taylor, Caitlin M. Dunning, Amanda L. Creech, Allison C. Warren, James M. McFarland, Mahdi Zamanighomi, Audrey Kauffmann, Nicolas Stransky, Marcin Imielinski, Yosef E. Maruvka, Andrew D. Cherniack, Aviad Tsherniak, Francisca Vazquez, Jacob D. Jaffe, Andrew A. Lane, David M. Weinstock, Cory M. Johannessen, Michael P. Morrissey, Frank Stegmeier, Robert Schlegel, William C. Hahn, Gad Getz, Gordon B. Mills, Jesse S. Boehm, Todd R. Golub, Levi A. Garraway, and William R. Sellers. Next-generation characterization of the Cancer Cell Line Encyclopedia. *Nature*, 569:503–508, 2019. doi: 10.1038/s41586-019-1186-3.
- [22] Andrew D. Rouillard, Gregory W. Gundersen, Nicolas F. Fernandez, Zichen Wang, Caroline D. Monteiro, Michael G. McDermott, and Avi Ma’ayan. The harmonizome: a collection of

- processed datasets gathered to serve and mine knowledge about genes and proteins. *Database*, 2016:baw100, 2016. doi: 10.1093/database/baw100.
- [23] Brinton Seashore-Ludlow, Matthew G. Rees, Jaime H. Cheah, Murat Cokol, Edmund V. Price, Matthew E. Coletti, Victor Jones, Nicole E. Bodycombe, Christian K. Soule, Joshua Gould, Benjamin Alexander, Ava Li, Philip Montgomery, Mathias J. Wawer, Nurdan Kuru, Joanne D. Kotz, C. Suk-Yee Hon, Benito Munoz, Ted Liefeld, Vlado Dančák, Joshua A. Bittker, Michelle Palmer, James E. Bradner, Alykhan F. Shamji, Paul A. Clemons, and Stuart L. Schreiber. Harnessing connectivity in a large-scale small-molecule sensitivity dataset. *Cancer Discov.*, 5: 1210–1223, 2015. doi: 10.1158/2159-8290.CD-15-0235.
- [24] Steven M. Corsello, Rohith T. Nagari, Ryan D. Spangler, Jordan Rossen, Mustafa Kocak, Jordan G. Bryan, Ranad Humeidi, David Peck, Xiaoyun Wu, Andrew A. Tang, Vickie M. Wang, Samantha A. Bender, Evan Lemire, Rajiv Narayan, Philip Montgomery, Uri Ben-David, Colin W. Garvie, Yejia Chen, Matthew G. Rees, Nicholas J. Lyons, James M. McFarland, Bang T. Wong, Li Wang, Nancy Dumont, Patrick J. O’Hearn, Eric Stefan, John G. Doench, Caitlin N. Harrington, Heidi Greulich, Matthew Meyerson, Francisca Vazquez, Aravind Subramanian, Jennifer A. Roth, Joshua A. Bittker, Jesse S. Boehm, Christopher C. Mader, Aviad Tsherniak, and Todd R. Golub. Discovering the anticancer potential of non-oncology drugs by systematic viability profiling. *Nat. Cancer*, 1:235–248, 2020. doi: 10.1038/s43018-019-0018-6.
- [25] Ashish Vaswani, Noam Shazeer, Niki Parmar, Jakob Uszkoreit, Llion Jones, Aidan N. Gomez, Łukasz Kaiser, and Illia Polosukhin. Attention is all you need. In *Adv. Neural Inf. Process. Syst.*, volume 30, 2017.
- [26] Chayaporn Suphavitai, Denis Bertrand, and Niranjana Nagarajan. Predicting cancer drug response using a recommender system. *Bioinformatics*, 34:3907–3914, 2018. doi: 10.1093/bioinformatics/bty452.
- [27] Lin Zhang, Xing Chen, Na-Na Guan, Hui Liu, and Jian-Qiang Li. A hybrid interpolation weighted collaborative filtering method for anti-cancer drug response prediction. *Front. Pharmacol.*, 9:1017, 2018. doi: 10.3389/fphar.2018.01017.

- [28] Guy W. Bemis and Mark A. Murcko. The properties of known drugs. 1. Molecular frameworks. *J. Med. Chem.*, 39:2887–2893, 1996. doi: 10.1021/jm9602928.

## Extended Data



**Extended Data Fig. 1 — Test-set checkpoint selection systematically inflates reported drug-blind performance.** **a**, Per-fold per-drug  $r$  on PASO’s 10-fold splits under fair evaluation with a validation holdout vs. the published protocol with test-set checkpoint selection. Per-drug  $r$  is largely unaffected ( $\Delta = +0.004$ ), because within-drug cell ranking is insensitive to the epoch that maximizes global  $r$ . **b**, Inflation decomposed on global  $r$ . Test-set snooping adds  $+0.042$  to the fair global  $r$  mean. Best-fold reporting adds  $+0.20$ , together reaching  $0.751$  and closely matching the published figure of  $0.745$ .

**Extended Data Table 1 — No drug representation improves within-drug cell ranking.** Ridge, 10-fold drug-blind CV, GDSC2. All conditions use  $n = 233$  drugs except LINCS ( $n = 104$ , LINCS-covered subset only). A random 2048-dimensional vector produces the same  $\Delta = +0.001$  as the real Morgan fingerprint, confirming that the small positive delta is a mechanical artifact of adding input dimensions under ridge regularization, not drug-specific signal.

Drug representation	Per-drug $r$	$\Delta$ vs. no drug
No drug features	$0.645 \pm 0.025$	—
Morgan fingerprint (ECFP4, 2048-bit)	$0.646 \pm 0.024$	+0.001
Random vector (2048-dim)	$0.646 \pm 0.024$	+0.001
Drug-target profile (binary, 5145 targets)	$0.646 \pm 0.024$	+0.001
LINCS perturbation signature (PCA-64)	0.665	+0.001
MoA one-hot (24 classes)	$0.645 \pm 0.025$	0.000

**Extended Data Table 2 — MoA as representation vs. distribution.** Per-drug  $r$  by condition. B vs. A tests whether MoA one-hot improves cell ranking ( $|\Delta| \leq 0.001$  uniformly). C vs. A tests whether MoA-weighted training improves cell ranking (large gains for signaling classes).

MoA class	A (no drug, uniform)	B (one-hot, uniform)	C (no drug, 20 $\times$ )	$\Delta(C-A)$
ERK MAPK signaling	0.427	0.428	0.673	+0.246
EGFR signaling	0.425	0.425	0.655	+0.230
Apoptosis regulation	0.524	0.524	0.547	+0.023
PI3K/MTOR signaling	0.610	0.610	0.703	+0.093
Genome integrity	0.742	0.742	0.747	+0.005
Overall	0.645	0.645	0.687	+0.042

**Extended Data Table 3 — Drug-feature null and  $K$ -shot matching replicate across independent datasets.** **a**, Morgan FP vs. no drug features, reporting per-drug  $r$  and  $\Delta$ . The null replicates in CTRPv2 and BeatAML. PRISM shows  $\Delta = +0.017$ , reflecting viability-based cytotoxicity rather than mechanism-specific sensitivity. **b**,  $K$ -shot matching generalizes to CTRPv2 but fails on PRISM due to drug-panel mismatch. BeatAML per-drug  $r$  rises from 0.453 at  $K = 0$  to 0.521 at  $K = 50$ .

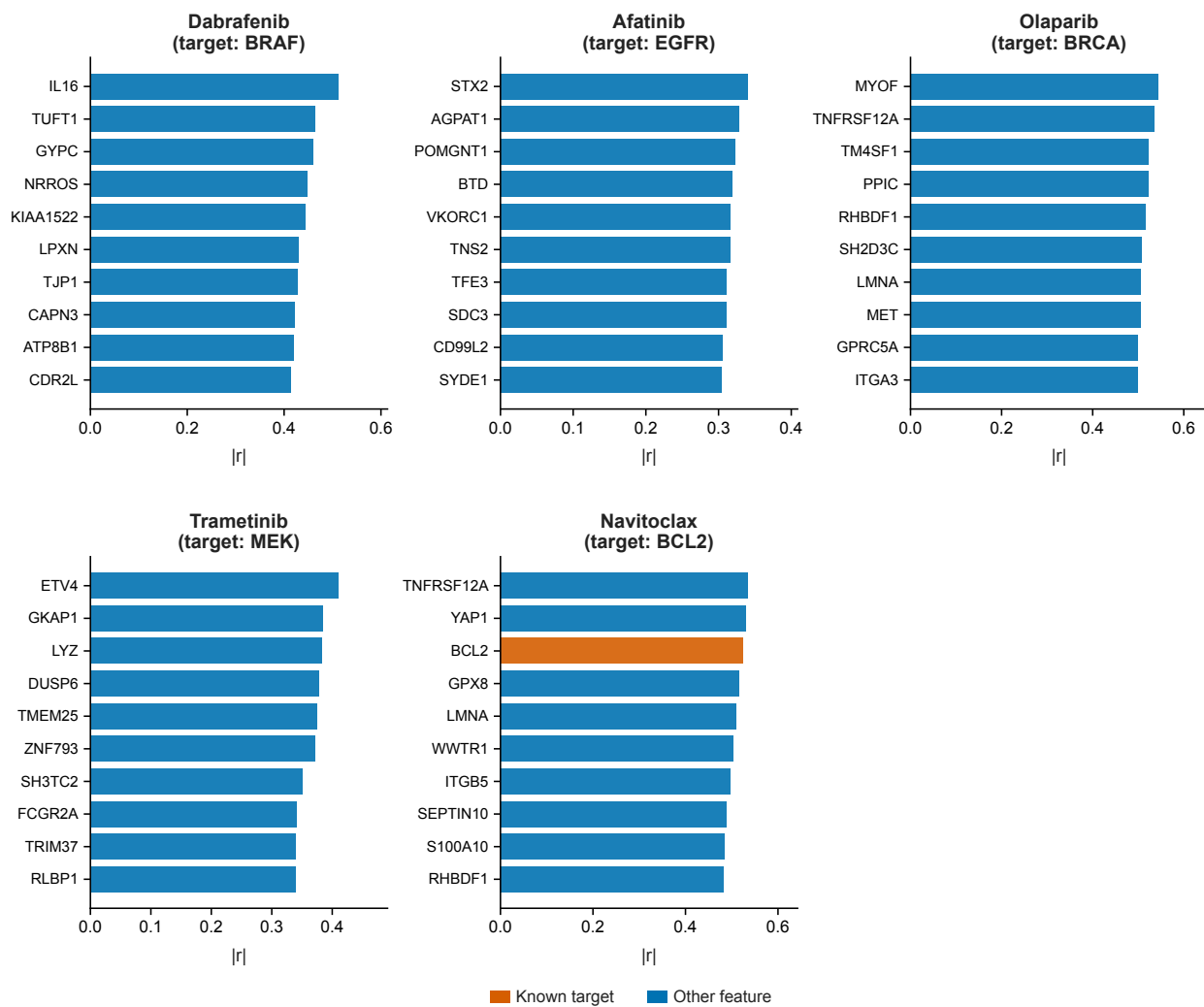
**a**

Dataset	No drug $r$	Morgan FP $r$	$\Delta$	$n_{\text{drugs}}$
GDSC2 (primary)	0.645	0.646	+0.001	233
CTRPv2	0.412	0.417	+0.005	545
BeatAML	0.453	0.454	+0.001	155
PRISM	0.117	0.134	+0.017	1079

**b**

Dataset	$K = 0$	$K = 1$	$K = 3$	$K = 10$	$K = 20$	$K = 50$
BeatAML	0.453	0.454	0.385	0.433	0.465	0.521
CTRPv2	0.411	0.416	0.314	0.325	0.379	0.463
PRISM	0.112	0.112	0.022	0.004	0.001	0.006

## Supplementary Information



**Supplementary Fig. 1 — Top-correlated features reflect lineage rather than chemical structure.** Top 10 most correlated features with  $IC_{50}$  for five targeted drugs. Orange bars indicate known molecular targets when present in the top 10. Only Navitoclax places its target (*BCL2*) in the top 10 (3rd). For the remaining four drugs, the known target ranks far below: *EGFR* ranks 29,348th for Afatinib, *BRAF* mutation ranks 9,944th for Dabrafenib. Lineage and cell-state markers dominate instead.

## Supplementary Note 1 — Formal decomposition of global Pearson $r$

Let  $y_{d,c}$  denote the true log IC<sub>50</sub> for drug  $d$  on cell line  $c$ , and  $\hat{y}_{d,c}$  the model prediction. Decompose each as a sum of a drug-level mean and a within-drug residual:

$$y_{d,c} = \bar{y}_d + \epsilon_{d,c}, \quad \hat{y}_{d,c} = \hat{\bar{y}}_d + \hat{\epsilon}_{d,c} \quad (\text{S1})$$

where  $\bar{y}_d = \frac{1}{|C_d|} \sum_c y_{d,c}$ .

**Covariance decomposition.** Expanding  $\text{Cov}(y, \hat{y})$ :

$$\text{Cov}(y, \hat{y}) = \text{Cov}(\bar{y}_d, \hat{\bar{y}}_d) + \underbrace{\text{Cov}(\bar{y}_d, \hat{\epsilon}_{d,c}) + \text{Cov}(\epsilon_{d,c}, \hat{\bar{y}}_d)}_{\text{cross-terms}} + \text{Cov}(\epsilon_{d,c}, \hat{\epsilon}_{d,c}) \quad (\text{S2})$$

When drug-level means and within-drug residuals are approximately uncorrelated in the model's predictions (the assumption holds when the model cannot predict drug-specific deviations), the cross-terms vanish, giving:

$$\text{Cov}(y, \hat{y}) \approx \underbrace{\text{Cov}(\bar{y}_d, \hat{\bar{y}}_d)}_{\alpha: \text{between-drug scale}} + \underbrace{\text{Cov}(\epsilon_{d,c}, \hat{\epsilon}_{d,c})}_{\beta: \text{within-drug ranking}} \quad (\text{S3})$$

**Variance decomposition.**  $\text{Var}(y) = \sigma_{\text{between}}^2 + \sigma_{\text{within}}^2$  where  $\sigma_{\text{between}}^2 = \text{Var}(\bar{y}_d)$  and  $\sigma_{\text{within}}^2 = \text{Var}(\epsilon_{d,c})$ .

**Global Pearson  $r$  as a weighted combination.** Let  $\omega_b = \sigma_{\text{between}}^{(y)} \sigma_{\text{between}}^{(\hat{y})} / (\sigma_y \sigma_{\hat{y}})$  and  $\omega_w = \sigma_{\text{within}}^{(y)} \sigma_{\text{within}}^{(\hat{y})} / (\sigma_y \sigma_{\hat{y}})$ , with  $\omega_b + \omega_w \leq 1$ . Then:

$$r_{\text{global}} \approx \omega_b r_{\text{between}} + \omega_w r_{\text{within}} \quad (\text{S4})$$

where  $r_{\text{between}} = \text{Cor}(\bar{y}_d, \hat{\bar{y}}_d)$  and  $r_{\text{within}} = \text{Cor}(\epsilon_{d,c}, \hat{\epsilon}_{d,c})$ .

**Why between-drug variance dominates in GDSC2.** Drug means  $\bar{y}_d$  in GDSC2 span  $[-5.2, +10.3] \ln \mu\text{M}$  (range 15.5 units), while within-drug standard deviations average  $\sim 1.5 \ln \mu\text{M}$ . Consequently  $\sigma_{\text{between}}^2 \gg \sigma_{\text{within}}^2$ , so  $\omega_b \gg \omega_w$  and global  $r$  is dominated by scale prediction accuracy. A model that predicts only drug means (DummyDrugAvg) achieves  $r_{\text{between}} = 1$  and  $r_{\text{within}} = 0$ , yet obtains high global  $r$ , the trivial predictor phenomenon<sup>5</sup>

**Per-drug  $r$  as an estimator of  $r_{\text{within}}$ .** The per-drug  $r$  defined in the main text (Pearson  $r$  within each test drug, averaged across drugs) is a direct estimator of  $r_{\text{within}}$ : by computing correlation within each drug independently, between-drug mean differences cancel.

**Empirical consistency.** Equation S4 predicts that a method improving  $r_{\text{between}}$  should increase global  $r$  without changing per-drug  $r$ . A method improving  $r_{\text{within}}$  should increase per-drug  $r$  with a smaller effect on global  $r$ , because  $\omega_w \ll \omega_b$ . LINCSeq signatures change global  $r$  by  $-0.058$  on the 104-drug LINCSeq-covered subset while per-drug  $r$  changes by  $+0.001$  (null), isolating the effect to between-drug scale prediction (here, a degradation rather than an improvement). Response matching at  $K = 50$  increases per-drug  $r$  by  $+0.056$  over the cell-mean prior without a corresponding global  $r$  increase, consistent with improving  $r_{\text{within}}$  only. These empirical results directly validate the decomposition.

## Supplementary Note 2 — Supporting results

### Baselines and performance ceilings

Table 1 contextualizes the per-drug  $r$  achieved by our methods against fundamental baselines and ceilings.

**Supplementary Table 1 — Per-drug  $r$  in context of baselines and measurement ceiling.** Methods are ordered by value. Dagger indicates response matching, which uses  $K$  pilot IC<sub>50</sub> measurements. All other methods are zero-shot.

Reference	Per-drug $r$	Notes
DummyDrugAvg (drug mean predictor)	0.000	Per-drug $r = 0$ by definition
Profile concordance (nearest-drug transfer baseline)	0.528	Mean across all 22 MoA classes (7 shown in Table 4)
Cell-mean prior (no observations)	0.645	86% of measurement ceiling
Response matching <sup>†</sup> ( $K = 50$ , blended, $N = 5$ )	<b>0.701</b>	$+0.056$ vs cell-mean, CV blend $w = 0.6$
Estimated within-assay replicate concordance	$\sim 0.754$	Within-protocol noise ceiling

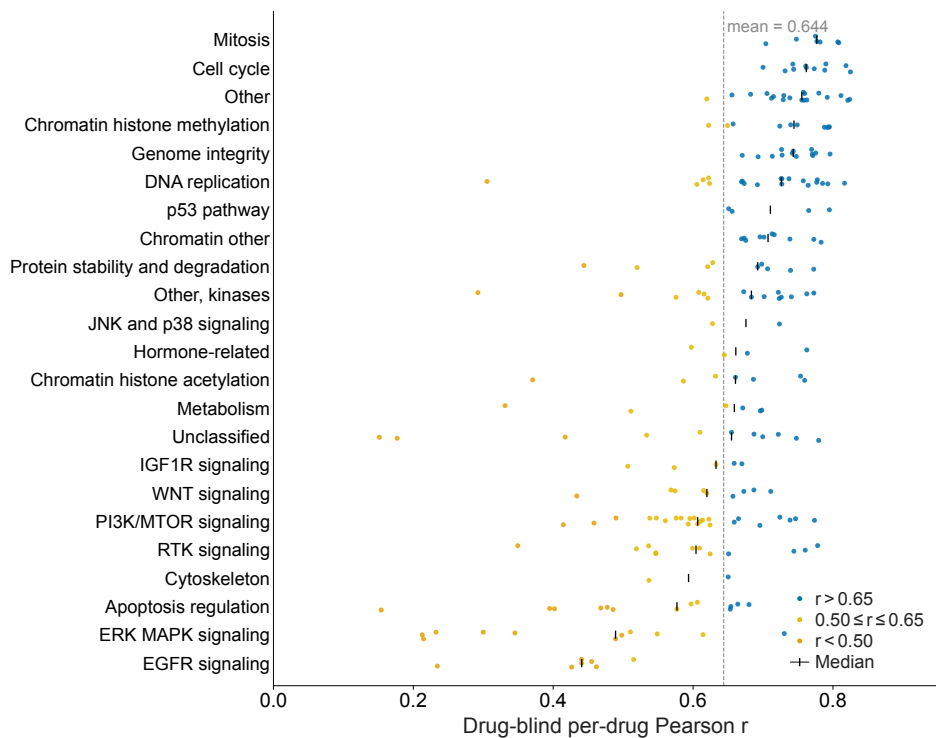
Table 2 shows ridge regression performance across evaluation settings. The counterintuitive reversal (cell-blind per-drug  $r <$  drug-blind) reflects that drug-blind retains all training cell lines, enabling strong cell-state ranking despite not knowing the drug identity.

### Per-drug performance by pathway

Drug-blind per-drug  $r$  varies substantially across drug pathway classes (Fig. 2).

**Supplementary Table 2 — Ridge regression performance by evaluation setting.** No drug features. Mixed-set is trivially easy (both drug and cell seen in training) and reported for reference only.

Evaluation setting	Global $r$	Per-drug $r$	Note
Mixed-set (random pair splits)	$\approx 0.89$	—	Trivial, drug and cell both in training
Cell-blind	$\approx 0.22$	0.438	
Drug-blind	$\approx 0.34$	0.645	Primary evaluation setting



**Supplementary Fig. 2 — Per-drug Pearson  $r$  by GDSC2 pathway annotation.** Blue,  $r > 0.65$ . Yellow,  $0.50 \leq r \leq 0.65$ . Orange,  $r < 0.50$ . Dashed line, overall mean.

**Supplementary Table 3 — Per-drug Pearson  $r$  by GDSC2 Target Pathway under all-drug training.** Ridge, RNA PCA-550 + mutation PCA-200, 10-fold drug-blind CV.

Target Pathway	Per-drug $r$ (mean $\pm$ s.d.)	$n$
Mitosis	0.772 $\pm$ 0.034	7
Cell cycle	0.767 $\pm$ 0.036	11
Genome integrity	0.742 $\pm$ 0.034	13
Chromatin histone methylation	0.731 $\pm$ 0.063	10
Chromatin other	0.714 $\pm$ 0.038	10
DNA replication	0.693 $\pm$ 0.109	20
Other, kinases	0.648 $\pm$ 0.120	15
WNT signaling	0.615 $\pm$ 0.079	9
PI3K/MTOR signaling	0.610 $\pm$ 0.088	23
IGF1R signaling	0.608 $\pm$ 0.061	5
RTK signaling	0.605 $\pm$ 0.116	12
Apoptosis regulation	0.524 $\pm$ 0.143	13
ERK MAPK signaling	0.427 $\pm$ 0.168	11
EGFR signaling	0.425 $\pm$ 0.082	7
Overall	0.645	233

The mean per-drug  $r$  delta (Morgan FP – no drug) of +0.001 is uniformly near zero across all 233 drugs (97% show  $|\Delta| \leq 0.01$ , range  $[-0.014, +0.018]$ ). Grouped by pathway class, even the largest pathway mean (+0.006 for RTK signaling) is  $9\times$  smaller than the  $K$ -shot gain at  $K = 50$ .

### Within-MoA training results and profile concordance

**Supplementary Table 4 — Within-class profile concordance and within-MoA training results.** Profile concordance is estimated from pairwise per-drug profile correlations within each MoA class. Within-MoA  $r$  uses leave-one-drug-out CV restricted to same-MoA drugs.

MoA class	$n$	All-drug $r$	Profile concordance	Within-MoA $r$
ERK MAPK signaling	11	0.427	0.565 $\pm$ 0.231	0.723
EGFR signaling	7	0.425	0.697 $\pm$ 0.051	0.799
PI3K/MTOR signaling	23	0.610	0.489 $\pm$ 0.147	0.702
RTK signaling	12	0.605	0.454 $\pm$ 0.142	0.640
Apoptosis regulation	13	0.524	0.331 $\pm$ 0.164	0.515 ( $\Delta = -0.009$ )
Genome integrity	13	0.742	0.570 $\pm$ 0.083	0.730
Mitosis	7	0.772	0.713 $\pm$ 0.090	0.788

For ERK MAPK and EGFR, within-MoA training recovers per-drug  $r$  that substantially exceeds the nearest-neighbor transfer baseline. Apoptosis regulation is unchanged ( $\Delta = -0.009$ ), reflecting a genuine biological limit.

## Supplementary Note 3 — Methods and robustness

### $K$ -shot blend calibration

**Supplementary Table 5** — CV-selected blend weight and per-drug  $r$  by  $K$ .  $w = 0$  corresponds to cell-mean prior only and  $w = 1$  to matching only. Permuted-drug control at  $K = 50$  yields  $r = 0.561$ .

$K$	CV blend weight ( $w$ )	Per-drug $r$	$\Delta$ vs. prior
0	—	0.645	—
1	0.1	0.645	0.000
3	0.0	0.645	0.000
5	0.1	0.646	+0.001
10	0.2	0.653	+0.008
20	0.3	0.670	+0.025
50	0.5–0.6	<b>0.701</b>	<b>+0.056</b>

### Cell representation alternatives

**Supplementary Table 6** — Cell representation alternatives all yield per-drug  $r \approx 0.645$ . Ridge, no drug features, 10-fold drug-blind PASO CV on GDSC2.

Cell representation	Dimensions	Per-drug $r$
RNA PCA(550) + mutation PCA(200) [baseline]	750	0.645
RNA PCA(1000) + mutation PCA(200)	1,200	0.645
KEGG pathway scores	1,284	0.645
RNA PCA(550) + pathway features	1,834	0.645
RNA PCA(100)	100	0.645
Pathway PCA(200)	200	0.645
Mutations PCA(200) only	200	0.645